

Nano-electric field sensor based on Two Dimensional Photonic Crystal resonator

R. Rajasekar^{a,*}, S. Robinson^b

^a Department of Electronics and Communication Engineering, Krishnasamy College of Engineering and Technology, Cuddalore, Tamil Nadu, India

^b Department of Electronics and Communication Engineering, Mount Zion College of Engineering and Technology, Pudukkottai, Tamil Nadu, India

ARTICLE INFO

Keywords:

Electric field sensor
Barium titanate
Photonic crystal resonator
Sensitivity

ABSTRACT

In this paper, hybrid Silicon-Barium Titanate (Si-BTO) based Two Dimensional Photonic Crystal (2DPC) platform is proposed for electric field sensing based on the effective refractive index modulation of electro-optic material. The nano-sensing platform is composed of the PC based resonator and inline quasi-waveguides in a 2D triangular lattice with circular rods that are arranged in the air medium. The BTO based nano-cavity resonator is playing a very important role in sensing the different electric field over a wide wavelength range. The operating wavelength range of the proposed sensor is investigated via Photonic Band Gap (PBG) which is obtained by the Plane Wave Expansion (PWE) method. The transmission efficiency, quality factor, electric field sensitivity and change in refractive index are analyzed by using Finite Difference Time Domain method (FDTD). The simulation results reveal that the resonant wavelength of the electric field sensor is linearly shifted to the higher wavelength region while increasing the electric field from 0 kV/mm to 25 kV/mm. The proposed sensing platform provides high transmission efficiency and very high refractive index sensitivity with an ultra-compact size. Hence, it is highly suitable for nano-chip based sensing applications.

1. Introduction

In recent years, ultra-compact photonic sensors are extremely attractive and excellent candidates for the optical community, and also it can meet the current demands such as lightweight, low power, ultra-compact size, high-precision and fast response for on-demand real-time applications [1]. The ultra-small electric field sensor is very important for voltage balancing, microwave detection, shielding of electromagnetic radiation, electromagnetic interference prevention, electric industry, detection of charges, radio-frequency reception, and so on [2,3]. Also, electric field sensors are attracted much attention due to their numerous advantages such as safety and remote measurement, intrinsically resistant to electromagnetic interference and rapid response speed [4]. In the literature, high sensitive, low power, highly accurate and ultra-compact photonic sensing platform has developed to detect the electric field for a wide range of application [5]. However, the optical losses are increased while reducing the size of the devices [6]. Alternatively, Photonic Crystals (PC) based devices are effectively utilized to reduce the device size to a nanoscale range with the ultra-low optical loss, and it provides strong photon confinement within the resonator [6].

PC is a kind of artificial nanostructure which is created by

periodically arranging the two different materials with different refractive index in a single substrate. The peculiar property of PC is Photonic Band Gap (PBG), which make it suitable for controlling and guiding the light signal at the scale of optical frequency [7]. The light signal in the PBG range is forbidden from propagating inside the structure. However, it can be allowed only by introducing the defects in the periodic PC structure. Fundamentally, the 2DPC platform is an excellent candidate for the optical device due to the simple structure, small size, perfect PBG calculation, strong light confinement and easy to integrate with optical integrated circuits [7]. Over the last two decade, 2DPC platform utilizes to design the various photonic devices such as logic gates [8], filters [9], demultiplexers [10], sensors [11–27] etc.

During the last decade, Si-based PC is a most promising platform for optical sensing applications. However, Si is insensitive to the external electric field and not suitable for electric field sensing because it has very low linear electro-optic coefficients due to their centrosymmetric crystalline structure [28]. Therefore, non-centrosymmetric crystalline structure based high-performance electro-optic material is integrated with Si to enhance the electro field sensitivity. Recent years, hybrid Si-LiNbO₃ based PC material is widely used for electric field sensor [29]. However, the LiNbO₃ electro-optic coefficients value ($r_{33} = 30 \text{ pm/V}$) only 20 times larger than Si and its integration very difficult with Si

* Corresponding author.

E-mail addresses: rajasekar8@gmail.com (R. Rajasekar), mail2robinson@gmail.com (S. Robinson).

chip [30]. As an alternative material, the nonlinear electro-optic material of Liquid Crystal (LC) and polymer ($r_{33} = 150 \text{ pm/V}$) infiltrated into the Si hole is employed to enhance the electric field and voltage sensitivity, respectively [26,27]. However, inserting LC and polymer in the Si hole is very difficult, and the LC extremely produces the slow optical response and it not suitable for photonic integration [31,32].

The challenges above are mitigated using BTO which has very high electro-optic coefficients ($r_{42} = 1640 \text{ pm/V}$) [33]. The integration of BTO with Si is very easy compared to other electric-optic material. Also, it produces high-speed responses and consumes less power owing to the use of electric field [34]. The refractive index difference between Si ($n = 3.5$) and BTO ($n = 2.4$) is very high, as a result, the light signal is strongly interacted within the photonic device and reduces their optical losses [35]. Hence, BTO is the excellent candidate and tremendously promising platform for PC based nano-optical devices.

In the literature, 2DPC based BTO platform is used to develop very few photonic devices. However, this platform is not utilized for electric field sensing application. Best of our knowledge, 2DPC based hybrid Si-BTO platform is first time proposed to sense the electric field with a good quality factor, high normalized transmission efficiency and high sensitivity with very low detection limit. The 2D-PWE and 2D-FDTD methods theoretically investigate the electric field sensor functional characteristics.

The rest of the paper is structured as follows. The electric field sensing principle discussed in Section 2. The PWE method is used to describe the PBG and structural parameters in Section 3. The photonic crystal resonator based sensor design focuses on Section 4. The functional characteristics evaluation discussed in Section 5. The electric field effect analysis and its sensing parameters optimization discussed in Section 6. At last, Section 7 concludes the paper.

2. Sensing principle

The working principle of electric field sensor is based on the electro-optic effect which means that the electric field is applied to change the refractive index of the electro-optic material (BTO). As a result, the resonant wavelength of the nanosensor will be shifted into the higher wavelength. The relationship between the refractive index of BTO and the electric field is expressed as [36].

$$n = n_0 + \frac{r_{eo} n_0^3}{2} E \quad (1)$$

$$E = V/L \quad (2)$$

where n_0 is the refractive index of BTO (2.289) at zero electric fields (0 kV/mm), r_{eo} is the electro-optic coefficient of BTO which is equal to 600 pm/V at 1550 nm wavelength [37]. L is the distance between two electrodes, and it is set to be 2 μm [36], V is the applied voltage, which should be below the breakdown voltage which is equal to 60 V for BTO [38] and E refers to the electric field. From equation (1) it is observed that for every 1 kV/mm electric field, the refractive index of BTO is increased by 0.003597.

3. Photonic band gap structure

Generally, in 2DPCs, the sensor can be realized by the square lattice or triangular lattice. The triangular lattice have the large bandgap, high filling factor, and less sensitive to structural parameters variation compared to the square lattice. Furthermore, a triangular lattice acts as a good platform for photonic integrated circuits and easily integrated with other nano-optical devices [39,40]. Also, the lattice may be in the form of dielectric rod type or air hole type (dielectric slab). The dielectric rods in air medium is preferred compared to the dielectric slab with hole type PCs due to their low optical losses, easy fabrication and defects based structure effectively produce single mode output [41].

The proposed electric field sensor design is based on 2DPC with the

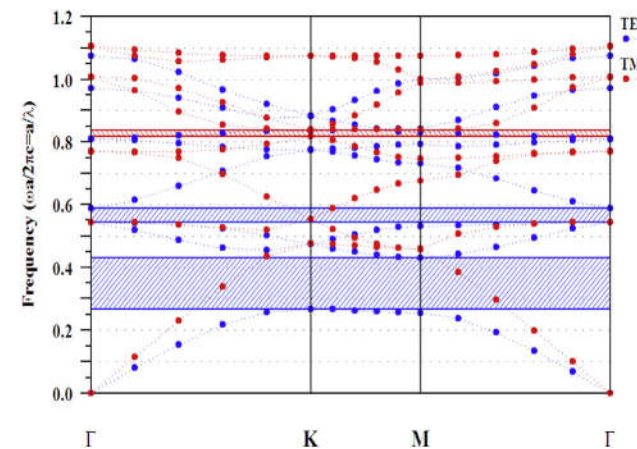


Fig. 1. Band diagram of a 27×21 perfect photonic crystal structure for a triangular lattice of silicon rods in air medium for TE and TM mode at $a = 630 \text{ nm}$ and $r = 130 \text{ nm}$. (For interpretation of the references to color in this figure legend, the reader is referred to the Web version of this article.)

triangular lattice of circular rods arranged in the air background. The periodic PC structure is composed of 27×21 circular rods arranged in X and Z directions, respectively. The Si refractive index is 3.5, the radius of the circular rod is 130 nm, and the lattice constant is selected to be 630 nm.

The proposed nano-electric field sensor TE and TM Photonic Band Gaps (PBG) are obtained by the Plane Wave Expansion (PWE) method using the aforementioned structural parameters. The triangular lattice of circular silicon rods in air platform-based perfect photonic crystal structure band diagram as shown in Fig. 1. From the Fig. 1, it is observed that the proposed nanostructure have two PBGs for TE polarization(blue color) and one PBG for TM polarization (red color). The first TE PBG (large bandgap)is accounted for electric field sensor design as its wavelength range covers low loss telecommunication wavelength, i.e., 1351.5 nm–2203.1 nm.

The proposed nanosensor structural parameters are accurately optimized by using gap map diagram as shown in Fig. 2(a)–(c). Fig. 2(a) shows the impact of PBG range with respect to the lattice constant. Fig. 2(a), it is observed that the bandgap frequency is shifted to the higher values while increasing the lattice constant. The optimum value of the lattice constant is selected as 630 nm, and it is highlighted by green color over the first TE PBG region.

The impact of PBG range while varying radius of the rod is shown in Fig. 2(b), by increasing the radius of the rod, the PBG frequency is shifted to the lower values. From this analysis, the radius of the rod as 130 nm is accounted for sensor design and it is highlighted by green color over the first TE PBG region. The refractive index of circular rods are silicon ($n = 3.5$), and the background index is air ($n = 1$). Hence, the refractive index difference between silicon and air is termed as delta ($\Delta = 2.5$). The delta value is represented by green color over the first TE PBG region, and its wavelength range lies between 1351.5 nm and 2203.1 nm. Fig. 2 (c), it is observed that the bandgap frequency is shifted to the lower values while increasing the delta.

4. Photonic crystal resonator

The Si-BTO coupled photonic crystal resonator based nano-electric field sensor layout structure is shown in Fig. 3 (a). The electric field sensing platform is composed of two inline quasi waveguides in the horizontal direction, and the BTO based PC resonator located between them. The inline quasi-waveguides are formed by line defect introduce to remove the Si rods in the input side and output side. The BTO based PC resonator is created by seven Si rods are (red color) removed to insert the three BTO rods (blue color) with a radius (r_b) of 300 nm and

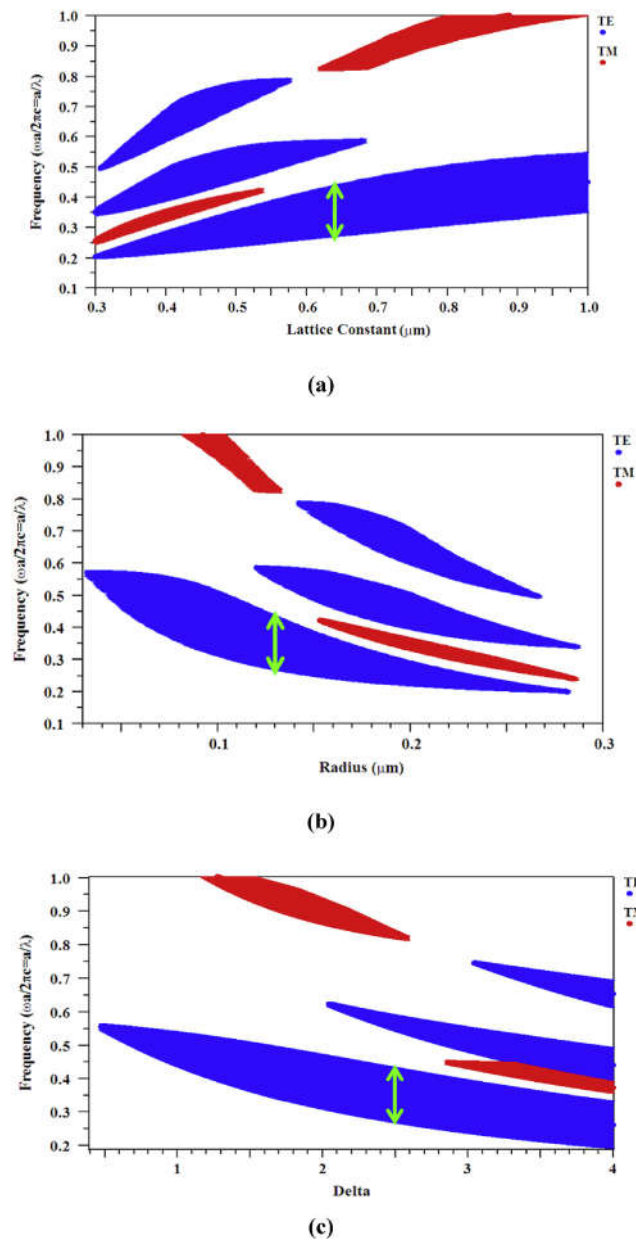


Fig. 2. Effect of gap map for circular dielectric rods in triangular lattice TM and TE PBG frequency variation with (a) lattice constant (b) radius and (c) delta.

the reaming four Si rods space created as nanocavity which is used to reduce their radiation loss. The two coupling rods (C) are placed in the inline quasi waveguides input and output side.

Fig. 3 (b) clearly shows the 3D view of Si-BTO coupled PC resonator based electric field sensor which shows the arrangement of Si and BTO rods in the triangular lattice structure and the proposed structure total chip area is $17 \mu\text{m} \times 11.4 \mu\text{m}$.

Fig. 4 shows the schematic configuration to sense the electric field using the nanoresonator coupled waveguide structure. The light source emits the Gaussian signal at first TE bandgap wavelength range from 1351.5 nm to 2203.1 nm. Then, the light signal is propagating through inline quasi-waveguide of the nanosensor, and this light signal is strongly coupled into BTO and nano-cavity at the resonant wavelength. In X-Z planes there are two electrodes placed to apply the external electric field to the BTO coupled PC resonator. As a result, the BTO refractive index is changed which shifts the resonant wavelength of the nanosensor. The resonant wavelength shift is observed by the time monitor which is located at the end of the nanosensor. The output light

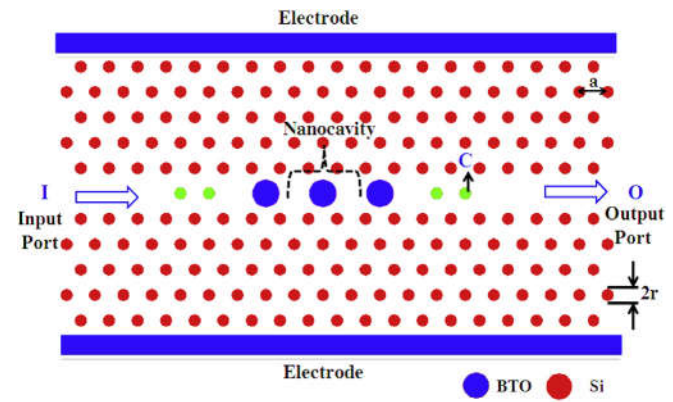


Fig. 3. (a) Layout structure of proposed Si-BTO coupled photonic crystal resonator based nano-electric field sensor with lattice constant $a = 630 \text{ nm}$, the radius of Si rods $r = 130 \text{ nm}$ and radius of BTO rods $r_b = 300 \text{ nm}$. (b) Three dimensional (3D) view of proposed nano-electric field sensor.

is transmitted to the photodetector, and it is used to detect the electrical signal. Finally, the detected signals are converted into the readable form by using a look-up table which is displayed on the computer.

5. Evaluation of functional characteristics

The Gaussian light signal is launched from input port "I" then the signal is confined into BTO and nano-cavity at center peak wavelength, and its corresponding output detected at output port "O". The normalized output spectrum of the electric field sensor is obtained by applying a Fast Fourier Transform (FFT) of the Gaussian signal which is stored by the time monitor. The normalized output spectrum of the nanosensor is calculated by following formula

$$T(f) = \frac{1/2 \int \text{real}(p(f)^{\text{monitor}}) dS}{\text{SourcePower}} \quad (3)$$

where $T(f)$ is the normalized transmission as a function of frequency, $p(f)$ denotes Poynting vector and dS is the surface normal. Finally, the $T(f)$ is changed into the function of wavelength. The proposed nano-electric field sensor normalized output spectrum and electric field distribution are theoretically investigated by the 2D-FDTD method. The normalized output spectrum of the nano-sensor without external electric field (0 kV/mm) is shown in Fig. 5. From the Fig. 5, the resonant wavelength of the proposed nano-electric field sensor is 1551 nm with the transmission efficiency of 98% is observed, and its corresponding electric field distribution is inserted in the Fig. 5.

The performance of the sensor is calculated by the quality factor (Q) which is defined as the ratio of resonant wavelength to the wavelength change at Full Width Half Maximum (FWHM).

$$Q = \lambda / \Delta \lambda \quad (4)$$

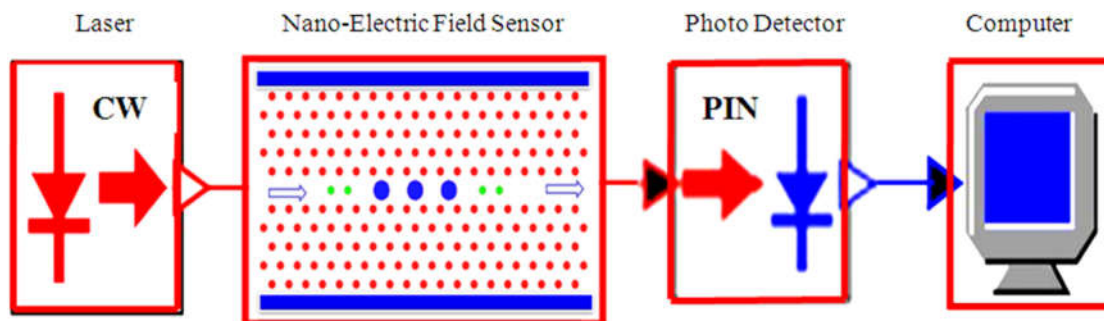


Fig. 4. Schematic structure of nano-electric field sensor based on hybrid Si-BTO based photonic crystal resonator.

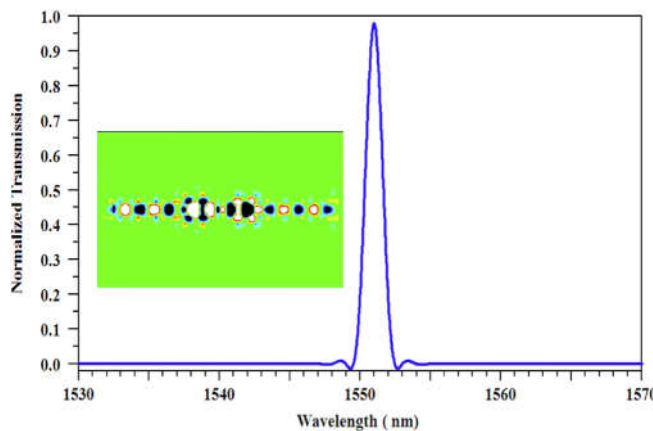


Fig. 5. Normalized transmission spectrum and electric field distribution (insert) of the photonic crystal resonator based nano-electric field sensor at without external electric field.

where λ is the resonant wavelength and $\Delta\lambda$ is the wavelength difference at FWHM. The quality factor of the proposed sensor is equal to 1410, which shows enhanced result than the existing sensor [11–25].

6. Electric field effect analysis

The ferroelectric material (BTO) refractive index is highly sensitive to the external electric field which is applied in the Z direction. Fig. 6 shows the nano-electric field sensor transmission spectrum for different applied electric field levels. The electric field effect on the proposed nanostructure is analyzed by increasing the electric field from 0 kV/mm to 25 kV/mm, and its equivalent transmission spectrum is used to

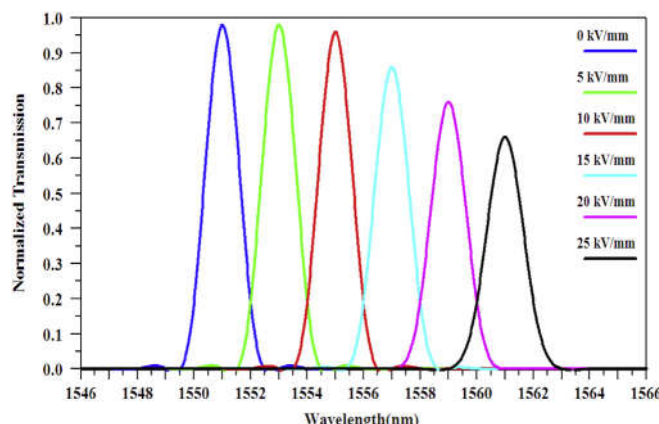


Fig. 6. Normalized resonant spectrum of photonic crystal resonator based nano-electric field sensor at the different external electric field from 0 kV/mm to 25 kV/mm with an increment of 5 kV/mm.

calculate the functional parameters of the nano-electric field sensor. When the applied electric field is changed from 0 kV/mm to 25 kV/mm with an increment of 5 kV/mm, the central wavelength of nano-resonator is linearly shifted to the higher wavelength. From the simulation result, it is noticed that the central wavelength of nanosensor is shifted around 10.13 nm for an applied electric field of 25 kV/mm. In addition, it is observed that the transmission efficiency of nanosensor is varied from 98% to 65.55% for an applied electric field increased from 0 kV/mm to 25 kV/mm.

The nano-resonator based electric field sensor property has been numerically calculated by the electric field sensitivity (S_E) which is defined as the ratio of change in the central wavelength owing to the applied electric field variation.

$$S_E = \Delta\lambda/\Delta E \quad (5)$$

where $\Delta\lambda$ is the resonant wavelength difference, and ΔE is the electric field difference. Generally, the electric field sensitivity should be high which means that the central wavelength of nanosensor is extremely shifted to higher wavelength due to minute electric field variation. In this attempt, the 2DPC resonator based nano-electric field sensor provides good electric field sensitivity which is equal to 0.4 nm per kV/mm. The functional parameters of the proposed nano-electric field sensor at different electric field levels are displayed in Table 1. The maximum transmission efficiency, quality factor, and sensitivity are 98%, 1420, and 0.407 nm/kV/mm, respectively.

The proposed electric field sensor is also used to detect the minimum electric field variation of 0.21 kV/mm, and its central wavelength has shifted by 0.1 nm compared with 0 kV/mm which is clearly shown in Fig. 7. The corresponding refractive index of 0 kV/mm and 0.21 kV/mm electric fields are 2.289000 and 2.289755, respectively. The following equation calculates the refractive index sensitivity (S_n) of nanosensor.

$$S_n = \Delta\lambda/\Delta n \quad (6)$$

where $\Delta\lambda$ represents the resonant wavelength difference, and Δn represents the refractive index difference. The obtained result shows that sensitivity is $S_n = 133.33 \text{ nm/RIU}$. The proposed nanosensor outputs as

Table 1

The functional parameters of the nano-electric field sensor at the different electric field level.

Electric Field level (kV/mm)	Refractive Index (RIU)	Resonant Wavelength (nm)	Transmission Efficiency (%)	Quality Factor	Electric Field Sensitivity (nm/kV/mm)
0	2.289000	1551.00	98.00	1410.00	Ref
5	2.306985	1553.00	98.00	1411.81	0.400
10	2.324970	1555.00	96.31	1413.63	0.400
15	2.342955	1557.10	86.29	1415.45	0.406
20	2.360940	1559.14	76.21	1417.27	0.407
25	2.378925	1561.15	66.13	1420.00	0.406

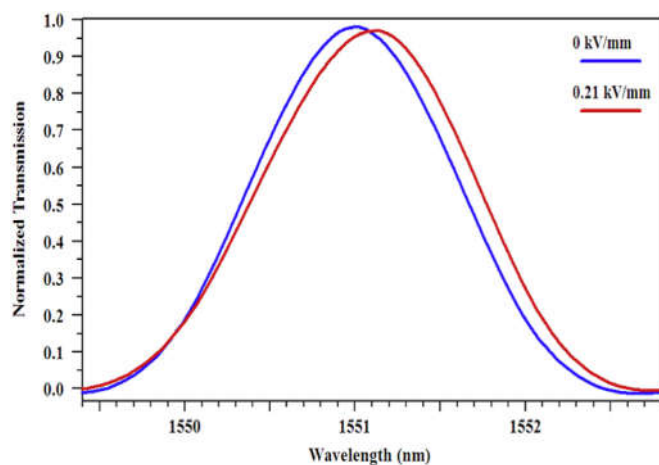


Fig. 7. The photonic crystal resonator based nano-electric field sensor resonant wavelength is shifted by a 0.21 kV/mm increase in the external electric field.

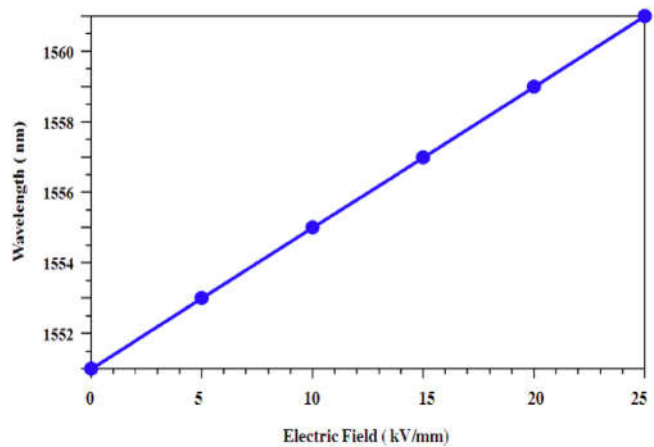


Fig. 8. The relationship between the resonant wavelength and the external electric field.

a function of the external electric fields as shown in Fig. 8. From the Fig. 8, it is observed that the nanosensor provide a good linear relationship between resonant wavelength shift and the external electric field. Also, the linear curve indicates that nano-electric field sensor provides wide dynamic range from 0 kV/mm to 25 kV/mm. Hence, the proposed nanosensor is extremely suitable for electric field sensing application.

6.1. Effect of ferroelectric rods

The number of ferroelectric rods (BTO) plays the important role for transmission efficiency, quality factor and sensitivity of nano-electric field sensor. The impact of a number of ferroelectric rods is analyzed by increasing the BTO rods from one to five with an increment of two BTO rods. The transmission efficiency and Q factor variations with the different number of BTO rods as shown in Fig. 9 and its corresponding functional parameters listed in Table 2. From Table 2, it is observed that nano-electric field sensor with three BTO rods provides high-quality factor and high transmission efficiency compared with one and five BTO rods. Therefore, the three BTO rods are accounted for electric field sensor design.

6.2. Effect of ferroelectric rod radius

The ferroelectric rod radius directly influences Q factor and transmission efficiency which is observed from the simulation result. The

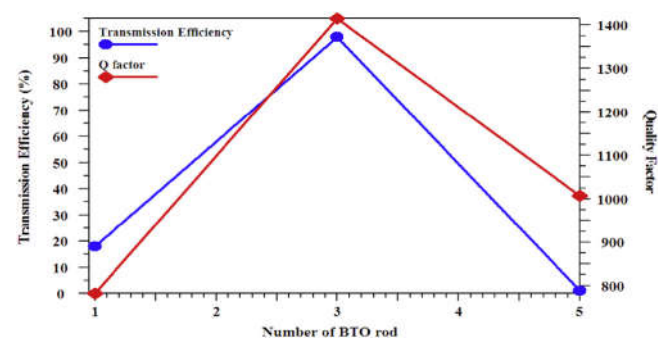


Fig. 9. The proposed nano-electric field sensor transmission efficiency and quality factor variations with the change of different number BTO rods.

Table 2

The functional parameters of the nanosensor at a different number of BTO rod.

Number of BTO rod	Resonant Wavelength (nm)	Transmission Efficiency (%)	Quality Factor
One	1564	18.00	0782.00
Three	1551	98.00	1410.00
Five	1550	01.00	1006.49

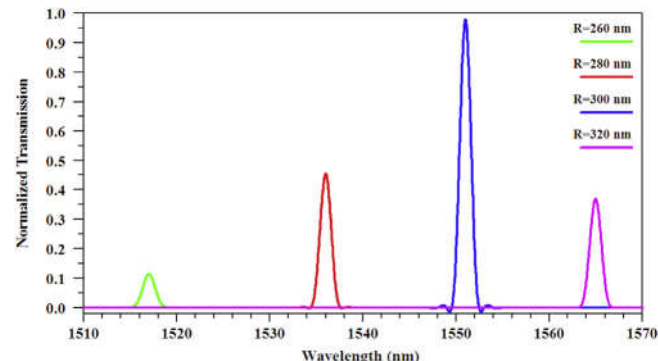


Fig. 10. The proposed nano-electric field sensor resonant wavelength and transmission efficiency variation with change in BTO rod radius from 260 nm to 320 nm with an increment of 20 nm.

Table 3

The functional parameters of the nanosensor at different BTO rod radius.

BTO rod Radius (nm)	Resonant Wavelength (nm)	Transmission Efficiency (%)	Quality Factor
260	1517	11.76	1264.16
280	1536	45.09	1280.30
300	1551	98.00	1410.00
320	1565	37.01	1304.16

BTO rod radius (r_b) is increased from 260 nm to 320 nm with an increment of 20 nm. The normalized output spectrum of the nano-electric field sensor at different ferroelectric rod radius is shown Fig.10 and its corresponding functional parameters listed in Table 3. From Table 3, it is observed that nano-electric field sensor with 300 nm radius provides high-quality factor and high transmission efficiency compared with other BTO rod radius. Therefore, the BTO rod radius of 300 nm is accounted for electric field sensor design.

6.3. Effect of nanocavity

Generally, the nanostructure-based 2DPC resonator in inline quasi-waveguide minimizes the coupling efficiency and increases the

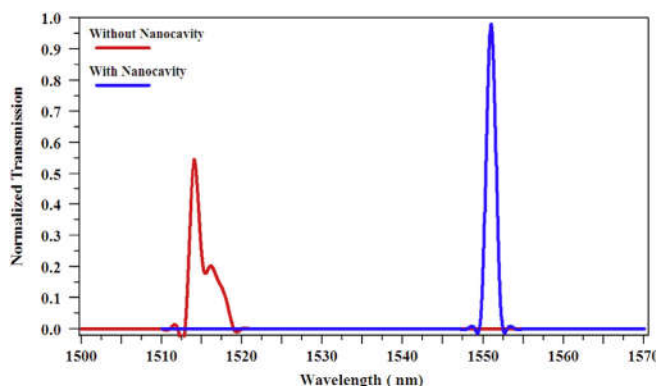


Fig. 11. The normalized transmission spectrum of the proposed photonic crystal resonator based nano-electric field sensor without and with nanocavity between the BTO rods.

radiation losses. It will lead to affect the quality factor and center wavelength of nano-sensor. Therefore, the nano-resonator coupled waveguide structure is optimized by introducing the nanocavity between ferroelectric rods. The normalized transmission spectrum of the PC resonator based electric field sensor without and with nanocavities shown Fig. 11.

The simulation results clearly show that the transmission efficiency (54.17%) and quality factor (1081) of the nanosensor without nanocavity become very low owing to the coupling loss and radiation losses are produced at the resonant wavelength. However, with nanocavity, the nanosensor coupling loss and radiation losses are minimized which in turn enhance the transmission efficiency (98%) and quality factor (1410) at the resonant wavelength.

6.4. Effect of coupling rods

The coupling rods (C) are mainly utilized to couple the light signal from input inline quasi-waveguide to nano-resonator which in turn to drop output inline quasi-waveguide at resonant condition. The number of coupling rods is properly selected to enhance the complete light signal transfer from inline quasi-waveguide to nano-resonator. If the number of coupling rods is not properly selected which decreases the transmission efficiency, quality factor and other optical parameters of nano-electric field sensor. Therefore, the optimum number of coupling rods is placed in the waveguides that are selected by increasing the coupling rods from one-one (input side-output side), two-two and three-three.

The Fig. 12 shows the normalized spectrum of electric field sensor at

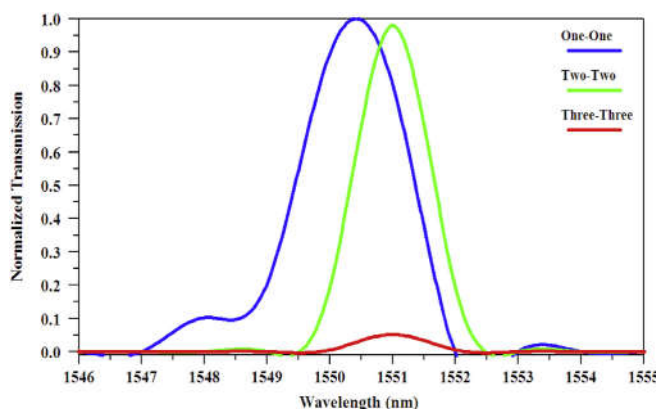


Fig. 12. The proposed nano-electric field sensor resonant wavelength, transmission efficiency and quality factor variation with a different number of coupling rods from one-one to three-three with an increment of one-one.

Table 4

The functional parameters of the nanosensor at a different number of coupling rod.

Number of coupling rod	Resonant Wavelength (nm)	Transmission Efficiency (%)	Quality Factor
One-One	1550.4	100.00	1264.16
Two-Two	1551.0	98.00	1410.00
Three-Three	1551.0	0.145	1034.00

a different number of coupling rods. The center wavelength, quality factor and transmission efficiency of nanostructures with three different numbers of coupling rods are listed in Table 4. From Table 4; it is identified that the two-two coupling rods provide good transmission efficiency (98%) and high-quality factor (1410) compared to one-one and three-three coupling rods.

6.5. Effect of different ferroelectric materials

In the literature, there are more than 500 ferroelectric materials are employed to develop the various optical and electronic components for real-time applications. These materials are generally categorized into four groups such as pyrochlore, perovskite oxides, bismuth layer and tungsten-bronze. Among all, the perovskite oxides are the most important one due to high piezoelectric effects, high pyroelectric coefficients, high ferroelectricity, high ferromagnetisms and strong electro-optic effects [34]. These properties are widely used in an electronic device and micro-optical system applications. Also, the perovskite oxides are highly suitable for thin film epitaxial integration which enhance the design flexibility of the photonic integrated circuit and reduces the production cost [42].

In recent years, there are very few perovskite oxides based ferroelectric materials such as Barium Titanate (BTO), Barium Strontium Titanate (BST), Lithium Niobate (LiNbO_3), Lithium Tantalate (LiTaO_3) and Lead Lanthanum Zirconate Titanate (PLZT) [42] are highly suitable as it is providing strong electro-optic response. Therefore, the aforementioned ferroelectric materials are integrated with photonic crystal silicon platform to enhance the sensitivity of the electric field sensor.

In this present work, five different materials have been considered to carry out the simulation, and its functional parameters such as the change in refractive index, resonant wavelength, transmission efficiency, quality factor and electric field sensitivity of the nano-electric field sensor are investigated while varying the applied electric field level. All the cases, the Si rod radius, the lattice constant, refractive index and ferroelectric material rod radius are kept as constant. However, the ferroelectric material, i.e., BTO, LiNbO_3 , LiTaO_3 , BST, and PLZT is changed in each case. The electric field effects of five different ferroelectric materials are analyzed by increasing the electric field from 0 kV/mm to 30 kV/mm with an increment of 15 kV/mm, and its respective functional characteristics are estimated and reported in Table 5. Fig. 13a–e shows the transmission spectrum of proposed nano-electric field sensor for different ferroelectric materials.

Table 6 shows the electric-optic material coefficient and maximum functional parameters of five different ferroelectric materials based nano-electric field sensor. From Table 6, it is observed that BTO based sensor provides high transmission efficiency (98%), high-quality factor (1421.06), detect very low electric field (0.21 kV/mm) and very high electric field sensitivity (0.4 nm/kV/mm) compared to other ferroelectric materials. Hence, in this attempt, hybrid Si-BTO based nanosensor is accounted for electric field sensing application.

The functional parameters such as transmission efficiency, quality factor, and refractive index sensitivity of the proposed sensor are compared with reported sensors which are displayed in Table 7. From this table, it is observed that L_3 nanocavity coupled PCW is designed with high-quality factor (3000). However, the refractive index

Table 5

Refractive index, resonant wavelength, transmission efficiency, quality factor and electric field sensitivity of five different ferroelectric materials for different electric field level.

Hybrid ferroelectric materials	Electric field level (kV/mm)	Refractive index(RIU) [37,43–47]	Resonant wavelength (nm)	Transmission efficiency (%)	Quality factor	Electric field sensitivity (nm/kV/mm)
BTO	0	2.2890	1551.00	98.00	1410.00	Ref
	15	2.3429	1557.10	86.29	1415.45	0.40
	30	2.3969	1563.17	56.13	1421.06	0.405
BST	0	2.2200	1540.80	71.98	1400.72	Ref
	15	2.2222	1541.10	74.02	1401.00	0.02
	30	2.2244	1541.40	74.97	1401.22	0.02
LiNbO ₃	0	2.2000	1538.00	58.44	1398.18	Ref
	15	2.2024	1538.30	59.41	1398.45	0.02
	30	2.2049	1538.60	60.51	1398.72	0.02
LiTaO ₃	0	2.1200	1525.50	20.26	1386.81	Ref
	15	2.1219	1525.80	21.09	1387.09	0.02
	30	2.1239	1526.10	21.74	1387.36	0.02
PLZT	0	2.4200	1566.00	43.51	1423.63	Ref
	15	2.4247	1566.60	40.96	1424.18	0.04
	30	2.4295	1567.20	39.48	1424.72	0.04

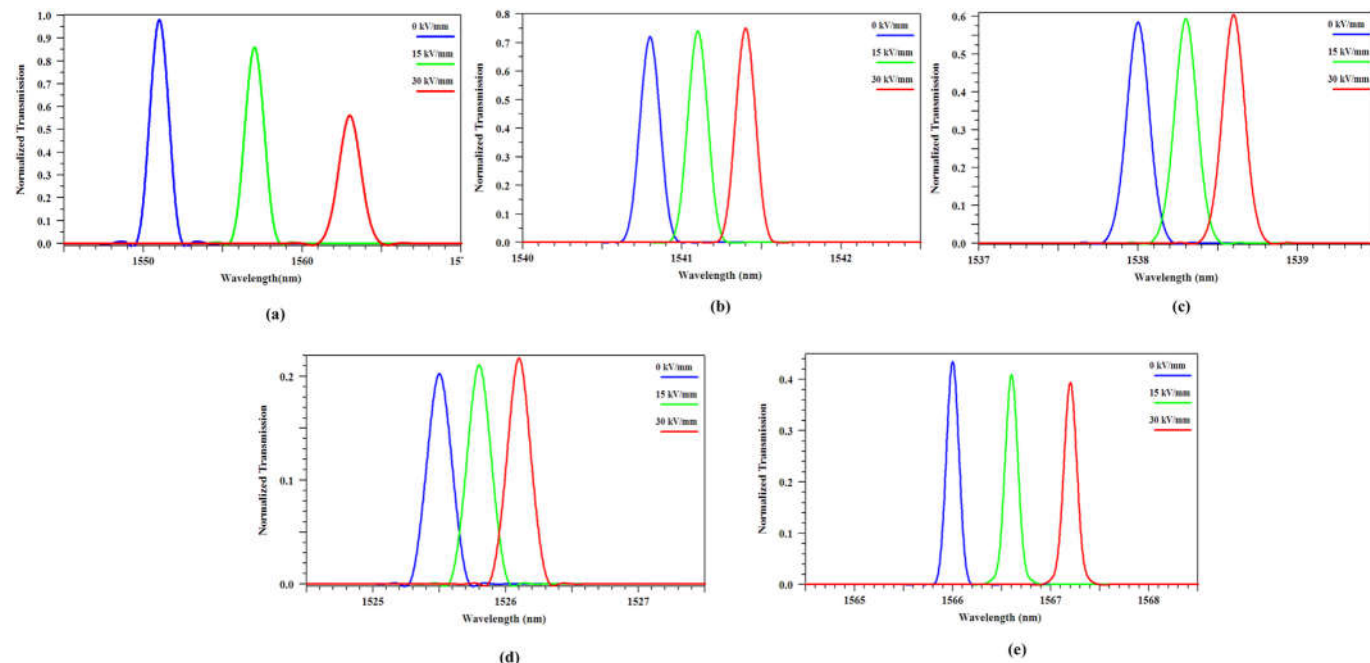


Fig. 13. The proposed nano-electric field sensor normalized transmission spectrum for (a) BTO (b) BST (c) LiNbO₃ (d) LiTaO₃ and (e) PLZT at different external electric field from 0 kV/mm to 30 kV/mm with an increment of 15 kV/mm.

Table 6

Electro-optic coefficient, maximum transmission efficiency, maximum quality factor, minimum detectable electric field and maximum electric field sensitivity of five different ferroelectric materials.

Ferroelectric materials	Electro optic coefficient (pm/V) [37,43–47]	Maximum transmission efficiency (%)	Maximum quality factor	Minimum detectable electric field (kV/mm)	Maximum electric field sensitivity (nm/kV/mm)
BTO	600	98.00	1421.06	0.21	0.405
BST	27.0	74.97	1401.22	7.2	0.02
LiNbO ₃	30.8	60.51	1398.72	6.8	0.02
LiTaO ₃	27.4	21.74	1387.36	7.4	0.02
PLZT	45.0	43.51	1424.72	3.4	0.04

sensitivity is very low (63 nm/RIU). The rhombic ring resonator provides high refractive index sensitivity (1000 nm/RIU) and high transmission efficiency (100%). However, the quality factor is very low (178).

From this analysis, it clear that the proposed nanocavity coupled resonator provides high transmission efficiency (98%), good quality factor (1420) and good refractive index sensitivity (133.33 nm/RIU)

with very low detection limit 7.5×10^{-4} compared to reported sensors. Hence, the proposed sensor is highly suitable for real-time applications.

7. Conclusion

In this attempt, a nanostructure-based photonic crystal resonator provides the ultra-compact platform for electric field sensing. The

Table 7

Comparison of designed nanosensor with the previously reported sensors.

Reference	Type of Sensing System	Transmission Efficiency (%)	Quality Factor	Refractive Index Sensitivity(nm/RIU)
[14]	Rhombic ring resonator	100.00	178.00	1000
[16]	Diamond ring resonator	****	1110.4	6.57
[17]	Circular ring resonator	99.50	477.83	72.27
[18]	Dual curve ring resonator	100.00	1550.0	4.172
[19]	Elliptical ring resonator	100.00	330.80	***
[20]	Modified L ₃ nancavaty	57.5	075.50	***
[21]	Paralleloid ring resonator	100.00	145.50	***
[22]	Optimized PC cavity	35.00	213.00	***
[23]	Inverted J-shaped cavity	***	394.87	8.86
[24]	Micro cavity coupled PCW	100.00	400.00	200
[25]	L ₃ cavity coupled PCW	***	3000	63
[25]	Nano cavity coupled PCW	***	400.00	155
Present Work	Nanocavity coupled PC resonator	98.00	1420.00	133.33

*** Not Discussed.

electro-optic effects of ferroelectric material play an important role in the electric field sensor. The BTO based PC resonator is coupled with inline quasi-waveguide causes narrow resonant in the transmission output spectrum which makes it feasible to sense the different electric field over a wide wavelength range. The nanosensor functional characteristics are analyzed by the FDTD method. The proposed nanoelectric field sensor offers a maximum quality factor equal to 1420, the sensitivity of 0.4 nm/kV/mm and dynamic range of about 0.21 kV/mm to 25 kV/mm. The maximum refractive index sensitivity of the proposed sensor is equal to 133.33 nm/RIU, and the detection limit is 7.5×10^{-4} . The total chip area of the proposed sensor is $17 \mu\text{m} \times 11.4 \mu\text{m}$. Hence, it is suitable for the electrical industry, integrated optics, NOEMS industry and nanotechnology-based sensing applications.

References

- [1] Tai-Ran Hsu, MEMS and Microsystems Design and Manufacture, second ed., McGraw-Hill Inc., New York, 2001.
- [2] O. Bottauscio, M. Chiampi, G. Crotti, D. Giordano, W.C. Wang, L. Zilberti, Uncertainty estimate associated with the electric field induced inside human bodies by unknown LF sources, *IEEE Trans. Instrum. Meas.* 62 (2013) 1436–1442.
- [3] T. Zhu, L. Zhou, M. Liu, J. Zhang, L. Shi, High sensitive space electric field sensing based on microfiber interferometer with field force driven gold nanofilm, *Sci. Rep.* 5 (2015) 15802.
- [4] C. Gutierrez-Martinez, J. Santos-Aguilar, Electric field sensing scheme based on matched LiNbO₃ electro-optic retarders, *IEEE Trans. Instrum. Meas.* 57 (2008) 1362–1368.
- [5] L. Chen, R.M. Reano, Compact electric field sensors based on indirect bonding of lithium niobate to silicon microrings, *Optic Express* 20 (2012) 4032–4038.
- [6] Z. Qiang, W. Zhou, R.A. Soref, Optical add-drop filters based on photonic crystal ring resonators, *Opt. Express* 15 (2007) 1823–1831.
- [7] J.D. Joannopoulos, P.R. Villeneuve, S. Fan, Photonic crystals: putting a new twist on light, *Nature* 386 (1997) 143–149.
- [8] E. Haq Shaik, N. Rangaswamy, Multi-mode interference-based photonic crystal logic gates with a simple structure and improved contrast ratio, *Photonic Netw. Commun.* 34 (2017) 140–148.
- [9] R. Rajasekar, S. Robinson, Trapezoid 2D photonic crystal nanoring resonator-based channel drop filter for WDM systems, *Photonic Netw. Commun.* (2018) 1–16.
- [10] K. Venkatachalam, S. Robinson, S.K. Dhamodharan, Performance analysis of an eight channel demultiplexer using a 2D-photonic crystal quasi square ring resonator, *Opto-Electron. Rev.* 25 (2017) 74–79.
- [11] R. Rajasekar, S. Robinson, Nano-pressure and temperature sensor based on hexagonal photonic crystal ring resonator, *Plasmonics* (2018) 1–13.
- [12] N.F.F. Aeed, M.F.O. Hameed, S.S.A. Obayya, Highly sensitive face-shaped label-free photonic crystal refractometer for glucose concentration monitoring, *Opt. Quant. Electron.* 49 (2017) 1–12.
- [13] M.S. Mohamed, M.F.O. Hameed, N.F.F. Aeed, M.M. El-Okr, S.S.A. Obayya, Analysis of highly sensitive photonic crystal biosensor for glucose monitoring, *J. ACES* 31 (2016) 836–842.
- [14] T. Suganya, S. Robinson, 2D Photonic crystal based biosensor using rhombic ring resonator for glucose monitoring, *J. microelectron.* 3 (2017) 349–353.
- [15] P. Sharma, P. Sharai, Design of photonic crystal based ring resonator for detection of different blood constituents, *Opt. Commun.* 348 (2015) 19–23.
- [16] H. Chopra, R.S. Kaler, B. Painam, Photonic crystal waveguide-based biosensor for detection of diseases, *J. Nanophotonics* 10 (2016) 036011.
- [17] S. Robinson, K.V. Shanthi, Analysis of protein concentration based on photonic crystal ring resonator, *Int. J. Opt. and Photonics* 10 (2016) 123–130.
- [18] S. Olyaei, A.M. Bahabady, A Two-curve-shaped biosensor using photonic crystal nano-ring resonators, *J. Nanostruct.* 4 (2014) 303–308.
- [19] R. Arunkumar, T. Suganya, S. Robinson, Design and analysis of photonic crystal elliptical ring resonator based pressure sensor, *J. Photon. Opt. Technol.* 3 (2017) 30–33.
- [20] K.V. Shanthi, S. Robinson, Two-dimensional photonic crystal based sensor for pressure sensing, *Photonic Sens.* 3 (2014) 248–253.
- [21] T. Suganya, S. Robinson, Design of 2D photonic crystal based force sensor using paralleloid Ring Resonator, *Microelectron* 3 (2017) 425–430.
- [22] A.K. Goyal, S. Pal, Design and simulation of high sensitive photonic crystal waveguide sensor, *Optik* 126 (2015) 240–243.
- [23] B. Painam, R.S. Kaler, M. Kumar, Active layer identification of photonic crystal waveguide biosensor chip for the detection of Escherichia coli, *Opt. Eng.* 55 (2016) 077105.
- [24] E. Chow, A. Grot, L.W. Mirkarimi, et al., Ultracompact biochemical sensor built with two-dimensional photonic crystal microcavity, *Opt. Lett.* 29 (2004) 1093–1095.
- [25] D.F. Dorfner, T. Hürlimann, T. Zabel, et al., Silicon photonic crystal nanostructures for refractive index sensing, *Appl. Phys. Lett.* 93 (2008) 181103.
- [26] D. Yang, H. Tian, Y. Ji, The study of electro-optical sensor based on slotted photonic crystal waveguide, *Opt. Commun.* 284 (2011) 4986–4990.
- [27] Y. Zhao, Y.N. Zhang, R.Q. Lv, J. Li, Electric field sensor based on photonic crystal cavity with Liquid crystal infiltration, *J. Lightwave Technol.* 35 (2017) 3440–3446.
- [28] J.F. Nye, Physical Properties of Crystals, Oxford University Press, New York, 1960.
- [29] T.W. Changa, C.J. Wu, Analysis of tuning in a photonic crystal multichannel filter containing coupled defects, *Optik* 124 (2013) 2028–2032.
- [30] S. Abel, T. Stoferle, C. Marchiori, C. Rossel, M. Rossell, R. Erni, D. Caimi, M. Sousa, A. Chelnokov, B. Offrein, J. Pompeyrene, A strong electro-optically active lead-free ferroelectric integrated on silicon, *Nat. Commun.* 4 (2013) 1671.
- [31] Y. Zhao, Y. Ying, Q. Wang, Latest research progress on methods and technologies for tunable photonic crystals, *Optic Laser. Technol.* 64 (2017) 278–287.
- [32] L. Kassa Baghdouche, T. Boumaza, M. Bouchamat, Optimization of Q-factor in nonlinear planar photonic crystal nanocavity incorporating hybrid silicon polymer material, *Phys. Scripta* 90 (2015) 065504.
- [33] P. Bernasconi, M. Zgonik, P. Gunter, Temperature dependence and dispersion of electro-optic and elasto-optic effect in perovskite crystals, *J. Appl. Phys.* 78 (1995) 2651–2658.
- [34] L.B. Kong, S. Li, T.S. Zhang, J.W. Zhai, F.Y.C. Boey, J. Mad, Electrically tunable dielectric materials and strategies to improve their performances, *Prog. Mater. Sci.* 55 (2010) 840–893.
- [35] T. Jin, L. Li, B. Zhang, H. Greg Lin, H. Wang, P. Lin, Real-time and label-free chemical sensor-on-a-chip using monolithic silicon-on-BaTiO₃ mid-infrared waveguides, *Sci. Rep.* 7 (2017) 5836.
- [36] P.T. Lin, Z. Liu, B.W. Wessels, Ferroelectric thin film photonic crystal waveguide and its electro-optic properties, *J. Opt. A-Pure. Appl. Opt.* 11 (2009) 075005.
- [37] D. Sun, X. Fu, H. Jiang, Simulations for dual-rail driven electro-optic modulators of BaTiO₃ crystal thin-film waveguides, *Optic Commun.* 301–302 (2013) 152–158.
- [38] Y. Watanabe, D. Sawamura, M. Okano, Recurrent local resistance breakdown of epitaxial BaTiO₃ heterostructure, *Appl. Phys. Lett.* 72 (1998) 2415.
- [39] C. Jamois, R. Wehrspohn, J. Schilling, F. Muller, R. Hillebrand, W. Hergert, Silicon-based photonic crystal slabs: two concepts, *IEEE J. Quant. Electron.* 38 (2002) 805–810.
- [40] A. Matthews, X.-H. Wang, Y. Kivshar, M. Gu, M, Band-gap properties of two-dimensional low-index photonic crystals, *Appl. Phys. B* 81 (2005) 189–192.
- [41] A.A.M. Kok, J.J.G.M. Van der Tol, R. Baets, M.K. Smit, Reduction of propagation loss in pillar-based photonic crystal waveguides, *J. Lightwave Technol.* 27 (2009) 3904–3911.
- [42] O. Nordseth, Ferroelectric Thin Films for Planar Photonic Device Applications, PhD Dissertation Dept. Electronics and telecommunication, NTNU, Trondheim, May 2010.
- [43] D.Y. Wang, K.P. Lor, K.K. Chung, H.P. Chan, K.S. Chiang, H.L.W. Chan, C.L. Choy, Mach-Zehnder electro-optic modulator based on epitaxial Ba_{0.7}Sr_{0.3}TiO₃ Thin Films, *Ferroelectrics* 357 (2007) 109–114.

- [44] K.L. Jim, C.W. Leung, H.L.W. Chan, Photonic crystal cavity embedded barium strontium titanate thin-film rib waveguide prepared by focused ion beam etching, *Thin Solid Films* 518 (2010) 101–103.
- [45] E.L. Wooten, K.M. Kiss, A. Yi-Yan, E.J. Murphy, et al., A review of lithium niobate modulators for fiber-optic communication systems, *IEEE J. Sel. Top. Quant. Electron.* 6 (2000) 69–82.
- [46] J.L. Casson, K.T. Gahagan, D.A. Scrymgeour, R.K. Jain, J.M. Robinson, V. Gopalan, R.K. Sander, Electro-optic coefficients of lithium tantalate at near-infrared wavelengths, *J. Opt. Soc. Am. B* 21 (2004) 1948–1952.
- [47] K. Nashimoto, PLZT thin film optical waveguide devices, *Proceedings of the 13th IEEE International Symposium on Applications of Ferroelectrics*, 2002, pp. 123–128.